

## Gravitomagnetic corrections on gravitational waves

This article has been downloaded from IOPscience. Please scroll down to see the full text article.

2010 Phys. Scr. 81 035008

(<http://iopscience.iop.org/1402-4896/81/3/035008>)

View [the table of contents for this issue](#), or go to the [journal homepage](#) for more

Download details:

IP Address: 192.135.36.27

The article was downloaded on 08/06/2010 at 16:50

Please note that [terms and conditions apply](#).

# Gravitomagnetic corrections on gravitational waves

S Capozziello, M De Laurentis, L Forte, F Garufi and L Milano

Dipartimento di Scienze Fisiche, Università di Napoli 'Federico II' and INFN Sezione di Napoli, Complesso Universitario di Monte Sant'Angelo, Edificio G, Via Cinthia, I-80126, Napoli, Italy

E-mail: [capozziello@na.infn.it](mailto:capozziello@na.infn.it)

Received 20 January 2010

Accepted for publication 20 January 2010

Published 2 March 2010

Online at [stacks.iop.org/PhysScr/81/035008](http://stacks.iop.org/PhysScr/81/035008)

## Abstract

Gravitational waveforms and production can be considerably affected by gravitomagnetic corrections considered in the relativistic theory of orbits. Besides the standard periastron effect of general relativity, new nutation effects arise when  $c^{-3}$  corrections are taken into account. Such corrections emerge as soon as matter-current densities and vector gravitational potentials cannot be discarded into dynamics. We study the gravitational waves (GWs) emitted through the capture, in the gravitational field of massive binary systems (e.g. a very massive black hole on which a stellar object is inspiralling) via the quadrupole approximation, considering precession and nutation effects. We present a numerical study to obtain GW luminosity, total energy output and gravitational radiation amplitude. From a crude estimate of the expected number of events toward peculiar targets (e.g. globular clusters) and, in particular, the rate of events per year for dense stellar clusters at the Galactic Center (Sagittarius region (SgrA\*)), we conclude that this type of capture could give signatures to be revealed by interferometric GW antennas, in particular by the forthcoming laser interferometer space antenna (LISA).

PACS numbers: 04.30.-w, 04.30.Tv, 95.85.Sz

(Some figures in this article are in colour only in the electronic version.)

## 1. Introduction

Searching for signatures of gravitational waves (GWs) and achieving a suitable classification of emitting sources have become two crucial tasks in GW science. In fact, today's sensitivity levels and theoretical developments are leading toward a general picture of GW phenomena that could not have been possible in the previous pioneering era. Experimentally, several GW ground-based laser interferometer detectors (10 Hz–10 kHz) have been built in the United States (LIGO) [1], Europe (VIRGO and GEO) [2, 3] and Japan (TAMA) [4], and are now taking data at designed sensitivities. A laser-interferometer space antenna (LISA) [5] ( $10^{-4}$ – $10^{-2}$  Hz) might fly within the next decade.

From a theoretical point of view, recent years have been characterized by numerous major advances due, essentially, to the development of numerical gravity. Concerning the most promising sources to be detected, the GW generation problem has improved significantly in relation to the dynamics of binary and multiple systems of compact objects such as

neutron stars and black holes (BHs). Besides, the problem of non-geodesic motion of particles in curved space-time has been developed considering the emission of GWs (and references therein) [6, 7]. Solving these problems is of considerable importance in order to predict the accurate waveforms of GWs emitted by extreme mass-ratio binaries, which are among the most promising sources for LISA [8].

From a more genuine astrophysical viewpoint, observations toward the central regions of galaxies have detected peculiar compact massive objects that are present in almost all observed galaxies. The occurrence of such systems has been revealed because of the advance in high angular resolution instrumentation for a wide range of electromagnetic wavelengths. Space telescopes such as HST or ground-based telescopes, which use adaptive optics, have been extremely useful for studying the kinematics of galactic internal regions reaching an accuracy of milli-pc for the Milky Way and of pc-fractions for external galaxies. The main conclusion of all these studies is that the central region of most galaxies is dominated by large compact objects with

masses of the order  $M \simeq 10^6\text{--}10^9 M_\odot$ . In the case of the Milky Way, the peculiar object in the Sagittarius region (SgrA\*) is of the order  $M \simeq 3 \times 10^6 M_\odot$  and is usually addressed as a massive black hole (MBH), even if its true physical nature is far from being finally identified [9, 10].

In any case, a deep link exists between the central MBH and the geometrical, kinematical and dynamical features of the host galaxy. In particular, the MBH is correlated with the global shape of the galactic spheroid, with the velocity dispersion of surrounding stars, with the mean density and the total mass of the host galaxy. The dynamics of stars moving around the MBH has a series of interesting characteristics that are of extreme interest for GW detection and production. Due to this occurrence, searching for GWs coming from objects interacting with MBHs is a major task for GW interferometry from space and ground-based experiments.

In this paper, we study the evolution of compact binary systems, formed through the capture of a moving (stellar) mass  $m$  by the gravitational field, whose source is a massive MBH of mass  $M$  where  $m \ll M$ . One expects that small compact objects ( $1\text{--}20 M_\odot$ ) from the surrounding stellar population will be captured by these black holes (BHs) following many-body scattering interactions at a relatively high rate [11, 12]. It is well known that the capture of stellar mass compact objects by massive MBHs could constitute, potentially, a very important target for LISA [13, 14]. However, dynamics has to be carefully discussed in order to consider and select all effects originating from standard stellar mass objects inspiralling over MBHs.

In a previous paper [15], we have shown that, in the relativistic weak field approximation, when considering higher-order corrections to the equations of motion, gravitomagnetic effects in the theory of orbits can be particularly significant, leading to chaotic behavior in the transient regime dividing stable from unstable trajectories. Generally, such contributions are discarded because they are considered too small. However, in a more accurate analysis, this is not true and gravitomagnetic corrections could give a peculiar characterization of dynamics.

In [15], the Newtonian and relativistic theories of orbits were reviewed considering, in particular, how relativistic corrections affect ‘classical’ orbits [17, 18]. Equations of motion and phase portraits of solutions indicate that, besides the standard periastron precession at order  $c^{-2}$ , new nutation effects appear at order  $c^{-3}$ , and it is misleading to neglect them.

According to these effects, orbits remain rather eccentric until the final plunge, and display both extreme relativistic perihelion precession and Lense–Thirring [19, 20] precession of the orbital plane due to the spin of the MBH, as well as orbital decay. In [21], it is illustrated how the measured GW waveforms can effectively map out the space-time geometry close to the MBH. In [22, 23], classical orbital motion (without relativistic corrections in the motion of the binary system) was studied in the extreme mass-ratio limit  $m \ll M$ , assuming stellar system density and richness as fundamental parameters. The following conclusions were made: (i) GW waveforms are characterized by orbital motion (in particular, closed or open orbits give rise to very different GW production and waveform shapes); (ii) in rich and dense stellar clusters,

a large production of GWs can be expected, so that these systems could be very interesting for the above-mentioned ground-based and space detectors; (iii) the amplitudes of the strongest GW signals are expected to be roughly an order of magnitude smaller than LISA’s instrumental noise.

In this paper, we investigate GW emission by binary systems, in the extreme mass-ratio limit, by the quadrupole approximation, considering orbits affected by both nutation and precession effects and taking into account also gravitomagnetic terms in the weak field approximation of the metric. We will see that GWs are emitted with a ‘peculiar’ signature related to orbital features: such a signature may be a ‘burst’ waveform with a maximum in correspondence to the periastron distance or a modulated waveform, according to orbit stability. Here we face this problem by discussing in detail the dynamics of such a phenomenon, which could greatly improve the statistics of possible GW sources.

Besides, we give estimates of the distributions of these sources and their parameters. It is worth noticing that the captures occur when objects in the dense stellar cusp surrounding a galactic MBH, undergo a close encounter, so that the trajectory becomes tight enough that orbital decay through emission of GWs dominates the subsequent evolution. According to [24, 25], for a typical capture, the initial orbital eccentricity is extremely large (typically  $1 - e \sim 10^{-6}\text{--}10^{-3}$ ) and the initial pericenter distance is very small ( $r_p \sim 8\text{--}100M$ , where  $M$  is the MBH mass [26]). The subsequent orbital evolution may (very roughly) be divided into three stages. In the first and longest stage the orbit is extremely eccentric, and GWs are emitted in short ‘pulses’ during pericenter passages. These GW pulses slowly remove energy and angular momentum from the system, and the orbit gradually shrinks and circularizes. After  $\sim 10^3\text{--}10^8$  years (depending on the two masses and the initial eccentricity) the evolution enters its second stage, where the orbit is sufficiently circular: the emission can be viewed as continuous. Finally, as the object reaches the last stable orbit, the adiabatic inspiral transits to a direct plunge, and the GW signal cuts off. Radiation reaction quickly circularizes the orbit over the inspiral phase; however, initial eccentricities are large enough that a substantial fraction of captures will maintain high eccentricity until the final plunge. It has been estimated [24] that about half of the captures will plunge with eccentricity  $e \gtrsim 0.2$ . While individually resolvable captures will mostly be detectable during the last  $\sim 1\text{--}100$  years of the second stage (depending on stellar mass  $m$  and MBH mass), radiation emitted during the first stage will contribute significantly to the confusion background. As we shall see, the above scenario is heavily modified since gravitomagnetic effects play a crucial role in modifying the orbital shapes that are far from being simply circular or elliptic and no longer closed. To be precise, standard relativistic corrections, such as periastron precession, give rise to non-closed orbits; however, in the case of gravitomagnetism, the occurrence of combined precession and nutation enhances the non-closure of orbits appearing, in principle, as a strong signature of the effect.

The layout of the paper is as follows. In section 2, we give a summary of gravitomagnetic corrections to the metric, showing how the geodesic equation is modified by their presence. Besides, we study in detail orbits with such

corrections, showing the phase portraits and velocity fields determined by the motion of mass  $m$  around the MBH. GW luminosity in the quadrupole approximation is discussed in section 3 while GW amplitude with gravitomagnetic corrections is discussed in section 4, giving also a resumé of numerical results. Rate and event number estimations are given in section 5. Conclusions are drawn in section 6.

## 2. Gravitomagnetic corrections

In a previous paper [15], we studied how the relativistic theory of orbits for massive point-like objects is affected by gravitomagnetic corrections. In particular, we considered the corrections on orbits of higher-order terms in  $v/c$ , and this is the main difference with respect to the standard gravitomagnetic effect discussed so far where corrections are taken into account only in the weak field limit and not on the geodesic motion. The problem of gravitomagnetic vector potential, entering into the off-diagonal components  $g_{0i}$  of the metric  $g_{\mu\nu}$ , can be greatly simplified and the corrections can be seen as further powers in the expansion in  $c^{-1}$  (up to  $c^{-3}$ ). Nevertheless, the effects on orbit behavior are interesting and involve not only precession at the periastron but also nutation corrections. Here we briefly recall such a previous result (see [15] for a detailed analysis).

The metric, in a weak field limit where gravitomagnetic corrections are present, is

$$ds^2 = \left(1 + \frac{2\Phi}{c^2}\right) c^2 dt^2 - \frac{8\delta_{ij} V^i}{c^3} c dt dx^j - \left(1 - \frac{2\Phi}{c^2}\right) \delta_{ij} dx^i dx^j, \quad (1)$$

where  $\Phi$  is the Newtonian potential and  $V^j$  is the gravitational vector potential (see [15] for details). It is clear that the approximation is up to  $c^{-3}$  in the Taylor expansion. From equation (1), it is straightforward to construct a variational principle from which the geodesic equation follows. Then we can derive the orbital equations. As a standard, we have

$$\ddot{x}^\alpha + \Gamma_{\mu\nu}^\alpha \dot{x}^\mu \dot{x}^\nu = 0, \quad (2)$$

where the dot indicates differentiation with respect to the affine parameter. In order to put in evidence the gravitomagnetic contributions, let us explicitly calculate the Christoffel symbols at lower orders. By some straightforward calculations, we obtain

$$\begin{aligned} \Gamma_{00}^0 &= 0, \\ \Gamma_{0j}^0 &= \frac{1}{c^2} \frac{\partial \Phi}{\partial x^j}, \\ \Gamma_{ij}^0 &= -\frac{2}{c^3} \left( \frac{\partial V^i}{\partial x^j} + \frac{\partial V^j}{\partial x^i} \right), \\ \Gamma_{00}^k &= \frac{1}{c^2} \frac{\partial \Phi}{\partial x^k}, \\ \Gamma_{0j}^k &= \frac{2}{c^3} \left( \frac{\partial V^k}{\partial x^j} - \frac{\partial V^j}{\partial x^k} \right), \\ \Gamma_{ij}^k &= -\frac{1}{c^2} \left( \frac{\partial \Phi}{\partial x^j} \delta_i^k + \frac{\partial \Phi}{\partial x^i} \delta_j^k - \frac{\partial \Phi}{\partial x^k} \delta_{ij} \right). \end{aligned} \quad (3)$$

In the approximation that we are going to consider, we retain terms up to orders  $\Phi/c^2$  and  $V^j/c^3$ . It is important

to point out that we discard terms such as  $(\Phi/c^4)\partial\Phi/\partial x^k$ ,  $(V^j/c^5)\partial\Phi/\partial x^k$ ,  $(\Phi/c^5)\partial V^k/\partial x^j$ ,  $(V^k/c^6)\partial V^j/\partial x^i$  and those of higher orders. Our aim is to show that, in several cases such as in tight binary stars, it is not correct to discard higher-order terms in  $v/c$  since physically interesting effects could arise. A vector equation for the spatial components of geodesics accounting for gravitomagnetic effects is [15]

$$\frac{d\mathbf{e}}{dl_{\text{euclid}}} = -\frac{2}{c^2} [\nabla\Phi - \mathbf{e}(\mathbf{e} \cdot \nabla\Phi)] + \frac{4}{c^3} [\mathbf{e} \wedge (\nabla \wedge \mathbf{V})]. \quad (4)$$

The gravitomagnetic term is the second in equation (4) and is usually discarded because it is not relevant. This is not true if  $v/c$  is quite large as in the cases of tight binary systems or point masses approaching BHs. Orbits corrected by such effects can be explicitly achieved.

### 2.1. Orbits with gravitomagnetic corrections

Orbits with gravitomagnetic effects can be obtained starting from classical theory and then correcting it by successive relativistic terms. In [15], it is shown that, taking into account gravitomagnetic terms, in the weak field approximation and in the extreme mass-ratio limit  $m \ll M$ , one obtains a motion with precession and nutation by solving the Euler–Lagrange equations numerically. It is possible to obtain parametric orbital equations of a massive particle starting from a variational principle where the canonical Lagrangian is derived by metric (1). With  $\frac{\partial \mathcal{L}}{\partial t} = 0$ , we have  $\frac{d}{dt} \left[ \frac{\partial \mathcal{L}}{\partial \dot{t}} \right] = 0$  and then  $\frac{\partial \mathcal{L}}{\partial \dot{t}} = E$ , where  $E$  is a constant that can be interpreted as an energy per mass unit. Owing to the dependence of the Lagrangian on  $\theta$  and  $\phi$ , we have, in general,  $\frac{\partial \mathcal{L}}{\partial \dot{\theta}} \neq 0$  and, furthermore, considering the initial conditions  $\theta = \frac{\pi}{2}$  and  $\dot{\theta} = 0$  we have  $\dot{\theta} \neq 0$ . This means, by straightforward calculations, a latitudinal motion in  $\theta$ , i.e. an orbital precession coupled with a nutation. On the other hand, planar motions are possible setting the initial condition  $\dot{r} = 0$ , i.e. for the particular case of circular orbits; otherwise orbital motions present precession and nutation corrections. Giving explicitly the energy first integral

$$\begin{aligned} i &= \frac{1}{c^3 r - 2cG\mu} \left\{ -4G\mu(\cos\theta + \sin\theta(\cos\phi + \sin\phi))\dot{r} \right. \\ &\quad \left. + r \left[ c^3 E - 4G\mu((-\sin\theta + \cos\theta(\cos\phi + \sin\phi))\dot{\theta} \right. \right. \\ &\quad \left. \left. + \sin\theta(\cos\phi - \sin\phi)\dot{\phi} \right] \right\} \end{aligned} \quad (5)$$

and the Euler–Lagrange equations (where the energy first integral can be suitably substituted), we obtain the differential system

$$\begin{aligned} \ddot{r} &= \frac{1}{cr(rc^2 + 2G\mu)} \left[ c(rc^2 + G\mu) (\dot{\theta}^2 + \sin^2\theta \dot{\phi}^2) r^2 \right. \\ &\quad \left. - 4G\mu i ((\cos\theta(\cos\phi + \sin\phi) - \sin\theta)\dot{\theta} \right. \\ &\quad \left. + \sin\theta(\cos\phi - \sin\phi)\dot{\phi}) r + cG\mu \dot{r}^2 - cG\mu i^2 \right], \quad (6) \\ \ddot{\phi} &= -\frac{2(c \cot\theta(rc^2 + 2G\mu)\dot{\theta}\dot{\phi}r^2 + \dot{r}(2G\mu \csc\theta(\sin\phi - \cos\phi)\dot{r} + cr(rc^2 + G\mu)\dot{\phi}))}{r^2(rc^3 + 2G\mu c)}, \end{aligned} \quad (7)$$

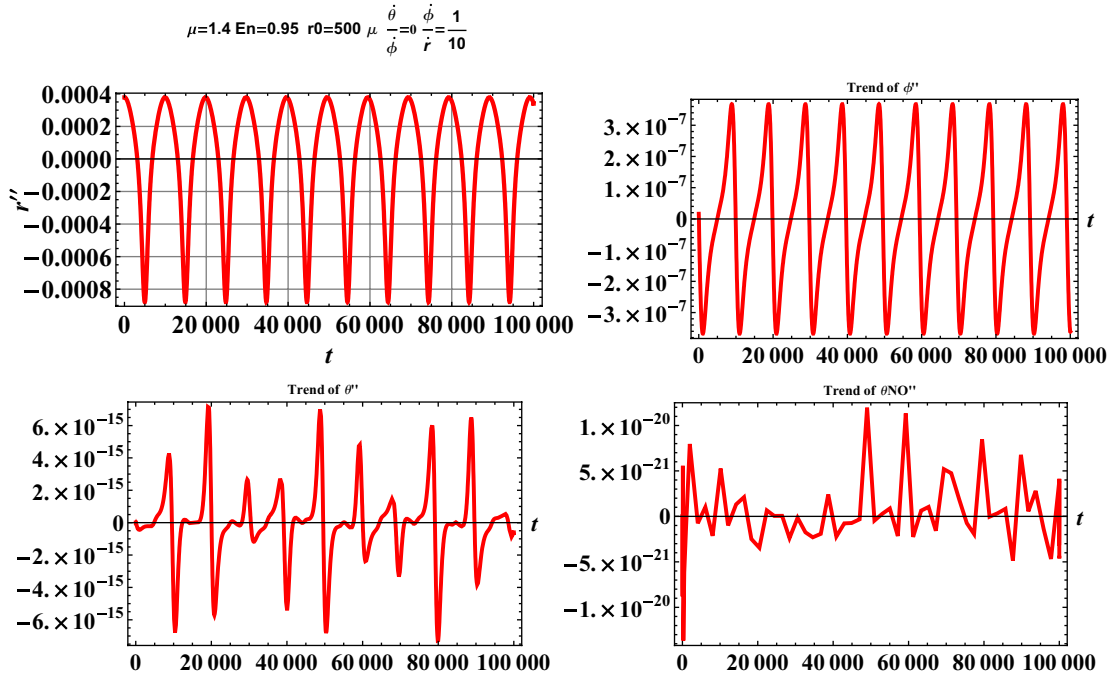


**Figure 1.** Plots of  $\ddot{r} = \ddot{r}(t)$  (left upper panel),  $\ddot{\phi} = \ddot{\phi}(t)$  (right upper panel),  $\ddot{\theta} = \ddot{\theta}(t)$  (left bottom panel) and  $\ddot{\theta}_{\text{NO}} = \ddot{\theta}_{\text{NO}}(t)$  (right bottom panel). As is seen, we have stiff equations owing to the turning points of the orbits. The example we show has been obtained by solving the system for the following parameters and initial conditions:  $\mu = 1.4M_{\odot}$ ,  $r_0 = 500\mu$ ,  $E = 0.95$ ,  $\phi_0 = 0$ ,  $\theta_0 = \frac{\pi}{2}$ ,  $\dot{\phi}_0 = -\frac{1}{10}\dot{r}_0$  and  $\dot{r}_0 = -\frac{1}{100}$ .

$$\ddot{\theta} = \frac{c \cos \theta r^2 (rc^2 + 2G\mu) \sin \theta \dot{\phi}^2 + \dot{r} (4G\mu (\cos \theta (\cos \phi + \sin \phi) - \sin \theta) \dot{t} - 2cr (rc^2 + G\mu) \dot{\theta})}{r^2 (rc^3 + 2G\mu c)}, \quad (8)$$

where  $\mu = \frac{mM}{m+M}$ . Following [15], it is worth noting that the vector potential  $V^j$  has disappeared from the equations of motion having been substituted by the effective quantity  $\Phi(r) \cdot v^j$  where  $\Phi \simeq \frac{G\mu}{r}$ .

Such a system is highly nonlinear. For its solution, we have to adopt numerical methods. The main characteristics of solutions can be deduced by a rapid inspection of figure 1.

As a first remark, we have to say that the above system of differential equations presents some difficulties since the equations are stiff and their numerical solution can diverge in several test points. Some numerical algorithms allow one to change the meshing dynamically in order to decrease the mesh size near the critical points.

For our purposes, we have found solutions by using the so-called *stiffness switching method* to provide an automatic tool of switching between a non-stiff and a stiff solver coupled with a more conventional explicit Runge–Kutta method for the non-stiff part of our differential equations.

We have used for the computation the sixth version of *Wolfram Software Mathematica* package [16]. The stiffness of the differential equations is evident from the figure, where the first and second derivatives of  $r$ , plotted with respect to  $t$ , show steep peaks corresponding to points where the radial velocity changes its sign abruptly. We show the time series of both  $\dot{r}(t)$  and  $r(t)$  together with the phase portrait  $\dot{r} = f(r)$  and  $\ddot{r}(t)$ , assuming given initial values for the angular precession and nutation velocities. The results for a given value of nutation angular velocity with a time span of 10 000 steps are shown. It is interesting to see that by increasing the initial nutation angular velocity, all the other initial conditions

remaining fixed, we obtain curves with decreasing frequencies for  $\dot{r}(t)$  and  $\ddot{r}(t)$ . This fact is relevant for an insight into orbital motion stability. The expected error in the phase of the orbit is of order  $10^{-16}$ . To show the orbital velocity field, we have performed a rotation and a projection of the orbits along the axes of maximal energy. In other words, by a *singular value decomposition* of de-trended positions and velocities, we have selected only eigenvectors corresponding to the largest eigenvalues and, of course, those representing the highest energy components.

The above differential equations for parametric orbital motion are nonlinear and with time-varying coefficients. In order to have a well-posed Cauchy problem, we have to define the initial and final boundary condition problems and the dynamical equilibrium of solutions (see the following pictures and numerical integrations).

From a physical point of view, equations (6)–(8) show additional terms with respect to classical Newtonian motion. Such corrections are dependent on  $\phi$  and  $\theta$ . Obviously, these terms become important as soon as the velocities approach relativistic regimes and the ratio  $v/c$  is quite large. In some physical situations, e.g. in extreme dense globular clusters or around the Galactic Center, such a ratio can be in the range  $10^{-2}$ – $10^{-3}$ , being not negligible at all (see [14] and references therein).

In figure 1, we have shown the trend of  $\dot{r}$ ,  $\dot{\phi}$ ,  $\dot{\theta}$ , as a function of  $t$ , and  $\ddot{\theta}_{\text{NO}}$ , which is the trend without gravitomagnetic correction. It can be seen that this last plot gives deviations from zero that are essentially null, confirming the planarity of orbital motions in the absence of gravitomagnetic corrections (the differences have at least four orders of magnitude between  $\ddot{\theta}_{\text{NO}}(t)$  and  $\ddot{\theta}(t)$ ).

For a further insight into the gravitomagnetic correction relevance on relativistic orbital motion, we have derived

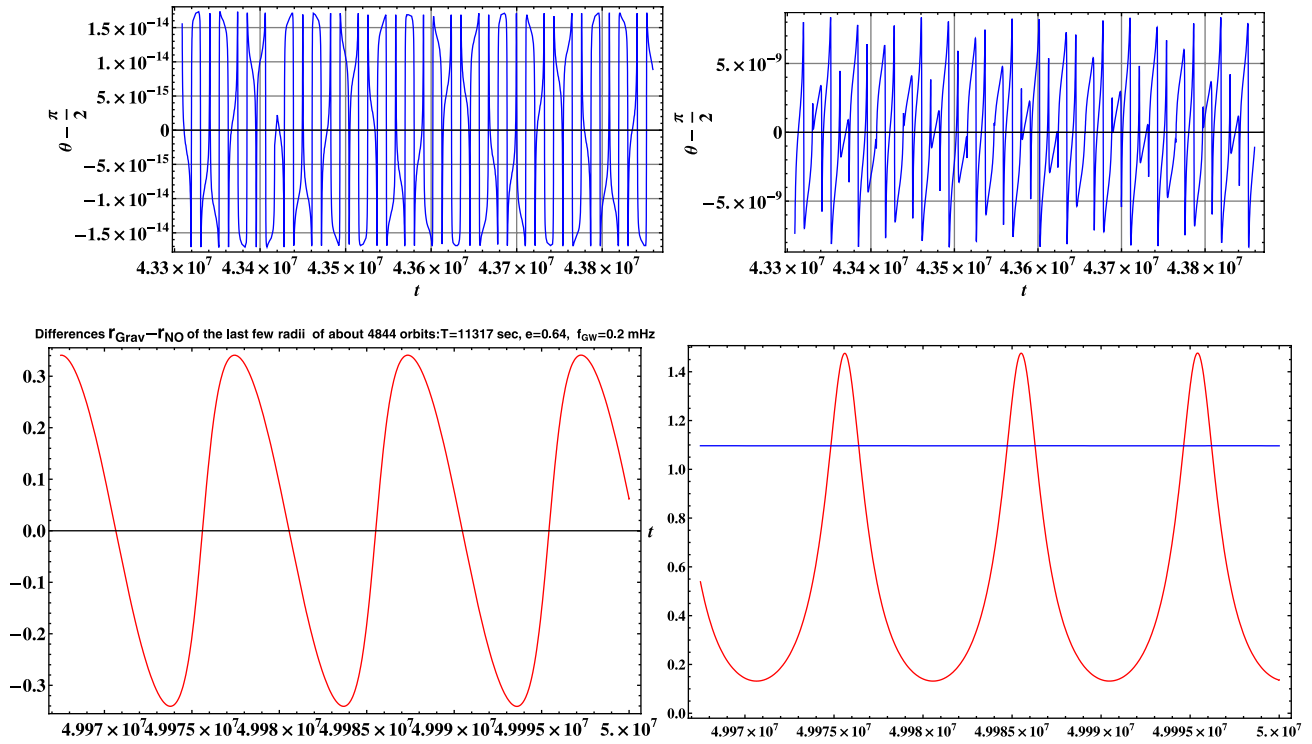


**Figure 2.** Plots of  $\theta_{\text{NO}}(t) - \frac{\pi}{2}$  (left upper panel) and  $\theta_{\text{Grav}}(t) - \frac{\pi}{2}$  (right upper panel). In the bottom panels,  $r_{\text{Grav}} - r_{\text{NO}}$  (left) and  $t_{\text{Grav}} - t_{\text{NO}}$  (right) are plotted (red lines). The ratio between coordinated time  $\frac{t_{\text{Grav}}}{\tau}$  versus proper time  $\tau$  is also plotted (blue line). The examples we show have been obtained by solving the system for the following parameters and initial conditions:  $\mu = 1.4M_{\odot}$ ,  $r_0 = 500\mu$ ,  $E = 0.95$ ,  $\phi_0 = 0$ ,  $\theta_0 = \frac{\pi}{2}$ ,  $\dot{\theta}_0 = 0$ ,  $\dot{\phi}_0 = -\frac{1}{10}\dot{r}_0$  and  $\dot{r}_0 = -\frac{1}{100}c$ .

a numerical solution with the following parameters and initial conditions:  $\mu \cong 1.4M_{\odot}$ ,  $r_0 = 500\mu$ ,  $E = 0.95$ ,  $\phi_0 = 0$ ,  $\theta_0 = \frac{\pi}{2}$ ,  $\dot{\phi}_0 = -\frac{1}{10}\dot{r}_0$  and  $\dot{r}_0 = -\frac{1}{100}c$ . In figure 2, we have plotted  $\theta_{\text{NO}}(t) - \frac{\pi}{2}$  without gravitomagnetic corrections and  $\theta_{\text{Grav}}(t) - \frac{\pi}{2}$  with gravitomagnetic corrections. In the bottom panel, there is, starting from the left to the right, the trend of the difference between the orbital radii  $r_{\text{Grav}}$  and  $r_{\text{NO}}$  with and without gravitomagnetic corrections respectively; we also plotted the differences  $r_{\text{Grav}} - r_{\text{NO}}$  and  $t_{\text{Grav}} - t_{\text{NO}}$  (red lines) and the ratio between coordinated time  $\frac{t_{\text{Grav}}}{\tau}$  versus proper time  $\tau$  (blue line). It is interesting to note the discrepancy from  $\frac{\pi}{2}$  of  $\theta$  with and without the gravitomagnetic effect. It is evident that we have planar orbital motion in the Newtonian case, while, in the presence of gravitomagnetic corrections, there is a tendency to precession and nutation of the orbital plane that give rise, orbit by orbit, to cumulative effects (a difference of five orders of magnitude between  $z_{\text{NO}}(t)$  and  $z_{\text{Grav}}(t)$  can be evaluated). At the beginning, the effect is very small but, orbit by orbit, it grows and, for a suitable interval of time, the effect cannot be neglected (see figure 3, left bottom panel in which the differences in  $x$  and  $y$  are shown starting from the initial orbits up to the last ones by a step of about 1500 orbits). On the bottom right the basic orbit is shown. For about 4850 orbits and a time interval of about 1.7 years, we found that the differences in coordinated time, computed with and without gravitomagnetic effects, are increasing as well as the differences in  $x$ ,  $y$  and  $z$  coordinates. See also figure 4, in which we show the differences between the GW dimensionless strain amplitude computed with and without gravitomagnetic orbital corrections (see the discussion in section 4).

### 3. GW luminosity in the quadrupole approximation

After the discussion of gravitomagnetic corrections to orbital motion, let us take into account the problem of how GW production and waveforms are affected by such effects. For this purpose, we have to consider the quadrupole approximation. This is, in our opinion, the best way of observing how gravitomagnetic effects correct GW luminosity and waveforms.

It is well known that the Einstein field equations give a description of how the curvature of space-time is related to the energy-momentum distribution. In the weak field approximation, moving massive objects produce GWs that propagate in vacuum with the speed of light. One can search for wave solutions, generated by a system of masses undergoing arbitrary motions, and then obtain the radiated power. The result, assuming that the source dimensions are very small with respect to the wavelengths (i.e. the quadrupole approximation [18]), is that the power  $\frac{dE}{d\Omega}$ , radiated in a solid angle  $\Omega$  with polarization  $e_{ij}$ , is

$$\frac{dE}{d\Omega} = \frac{G}{8\pi c^5} \left( \frac{d^3 Q_{ij}}{dt^3} e_{ij} \right)^2, \quad (9)$$

where  $Q_{ij}$  is the quadrupole mass tensor:

$$Q_{ij} = \sum_a m_a (3x_a^i x_a^j - \delta_{ij} r_a^2), \quad (10)$$

$r_a$  being the modulus of the vector radius of the  $a$ th particle and the sum running over all masses  $m_a$  in the system. We must note that the result is independent of the kind of stresses

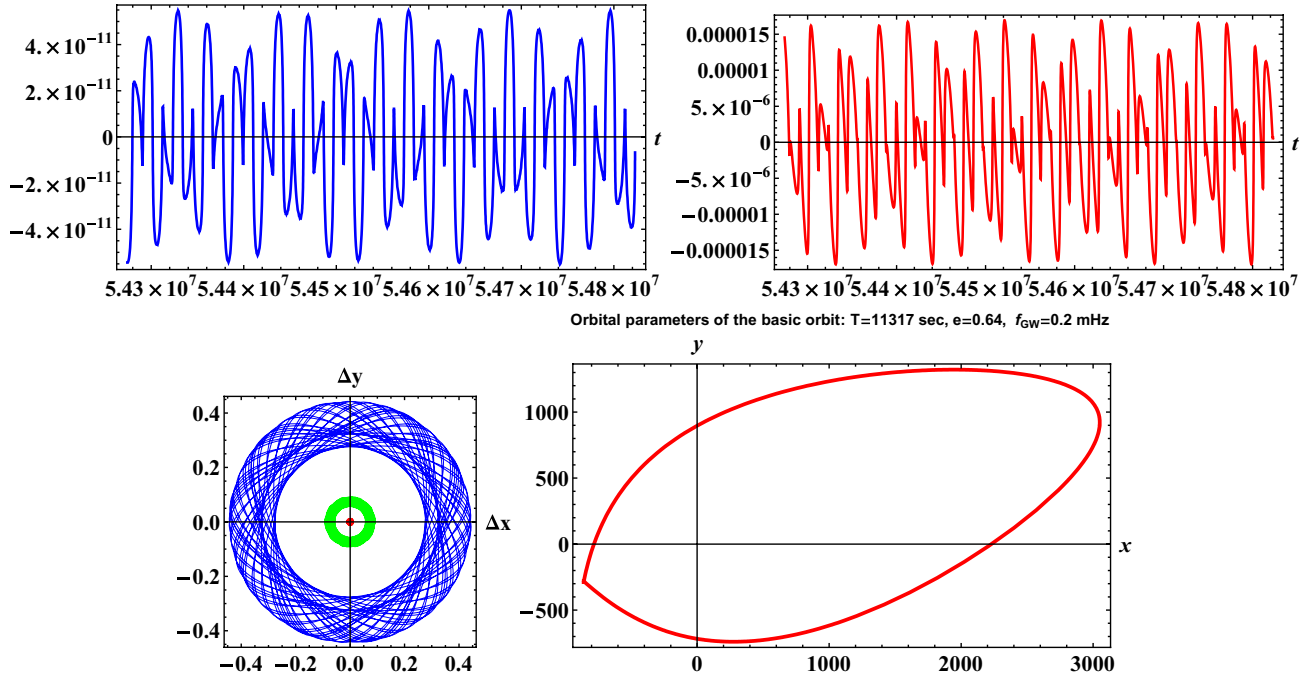


**Figure 3.** Plots of  $z_{\text{NO}}(t)$  (left upper panel) and  $z_{\text{Grav}}(t)$  (right upper panel). It is interesting to see differences of about five orders of magnitude between the two plots. At the beginning, the effect is very small but, orbit by orbit, it grows and, for a suitable interval of coordinated time, the effect cannot be neglected (see the left bottom panel, in which differences in  $x$  and  $y$ , starting from the initial orbits up to the last ones, by steps of about 1500 orbits, are reported). The internal red circle represents the beginning, the middle one is the intermediate situation (green) and the blue one is the final result of the correlation between  $\Delta x$  and  $\Delta y$ , with  $\Delta x = x_{\text{Grav}} - x_{\text{NO}}$  and  $\Delta y = y_{\text{Grav}} - y_{\text{NO}}$ . On the bottom right, the basic orbit is shown.

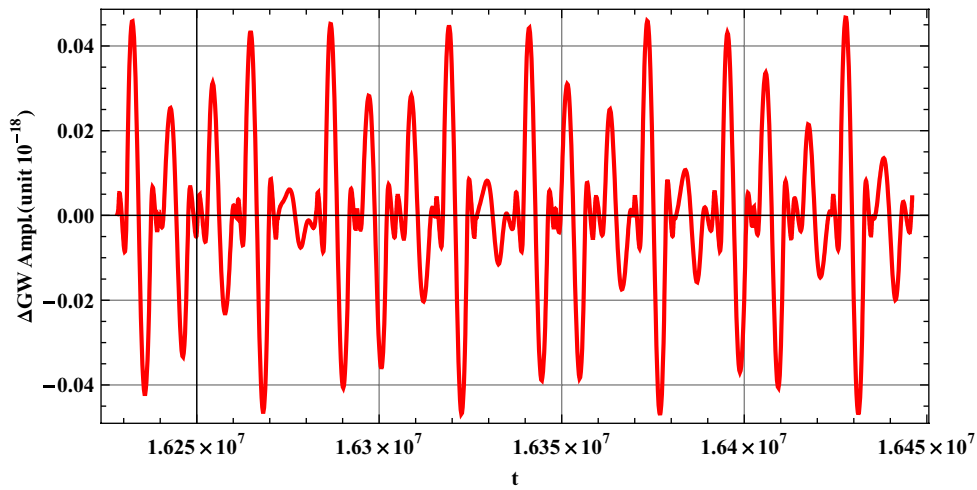


**Figure 4.** Plot of the differences of total gravitational waveform  $h$ , with and without gravitomagnetic orbital correction for a neutron star of  $1.4M_{\odot}$  orbiting around an MBH. The waveform was computed at the Earth-distance from SgrA\* (the central Galactic BH). The example we show has been obtained by solving the system for the following parameters and initial conditions:  $\mu \approx 1.4M_{\odot}$ ,  $r_0$ ,  $E = 0.95$ ,  $\phi_0 = 0$ ,  $\theta_0 = \frac{\pi}{2}$ ,  $\dot{\theta}_0 = 0$ ,  $\phi_0 = -\frac{1}{10}\dot{r}_0$  and  $\dot{r}_0 = -\frac{1}{100}$ . It is worth noting that frequency modulation gives cumulative effects after suitable long times.

present in dynamics. If one sums equation (9) over the two allowed polarizations, one obtains

$$\sum_{\text{pol}} \frac{dE}{d\Omega} = \frac{G}{8\pi c^5} \left[ \frac{d^3 Q_{ij}}{dt^3} \frac{d^3 Q_{ij}}{dt^3} - 2n_i \frac{d^3 Q_{ij}}{dt^3} n_k \frac{d^3 Q_{kj}}{dt^3} - \frac{1}{2} \left( \frac{d^3 Q_{ii}}{dt^3} \right)^2 + \frac{1}{2} \left( n_i n_j \frac{d^3 Q_{ij}}{dt^3} \right)^2 + \frac{d^3 Q_{ii}}{dt^3} n_j n_k \frac{d^3 Q_{jk}}{dt^3} \right], \quad (11)$$

where  $\hat{n}$  is the unit vector in the radiation direction. The total radiation rate is obtained by integrating equation (11) over all emission directions; the result is

$$P = \frac{dE}{d\Omega} = \frac{G}{c^5} \left( \frac{d^3 Q_{ij}}{dt^3} \frac{d^3 Q_{ij}}{dt^3} - \frac{1}{3} \frac{d^3 Q_{ii}}{dt^3} \frac{d^3 Q_{jj}}{dt^3} \right). \quad (12)$$

It is then possible to estimate the amount of energy emitted in the form of GWs from a system of massive interacting objects. In this case, the components of the quadrupole mass tensor are

$$\begin{aligned}
Q_{xx} &= \mu r^2 (3 \cos^2 \phi \sin^2 \theta - 1), \\
Q_{yy} &= \mu r^2 (3 \sin^2 \phi \sin^2 \theta - 1), \\
Q_{zz} &= \frac{1}{2} r^2 \mu (3 \cos 2\theta + 1), \\
Q_{xz} &= Q_{zx} = r^2 \mu \left( \frac{3}{2} \cos \phi \sin 2\theta \right), \\
Q_{yz} &= Q_{zy} = r^2 \mu \left( \frac{3}{2} \sin 2\theta \sin \phi \right), \\
Q_{xy} &= Q_{yx} = r^2 \mu \left( \frac{3}{2} \sin^2 \theta \sin 2\phi \right),
\end{aligned} \tag{13}$$

where the masses  $m_i$  have polar coordinates  $\{r_i \sin \theta \cos \phi, r_i \sin \theta \sin \phi, r_i \cos \theta\}$  and  $\mu$  is the reduced mass. The origin of the motions is taken at the center of mass. Such components can be differentiated with respect to time as in equation (12). The gravitomagnetic corrections affect, essentially, these quantities and, consequently, the GW amplitude  $h$  and the radiation rate  $P$ , as we will see below.

#### 4. GW amplitude with gravitomagnetic corrections

Direct signatures of gravitational radiation are given by GW amplitudes and waveforms. In other words, the identification of a GW signal is strictly related to the accurate selection of the waveform shape by interferometers or any possible detection tool. Such an achievement could give information on the nature of the GW source, the propagating medium and, in principle, the gravitational theory producing such a radiation [27].

Considering the formulas of the previous section, GW amplitude can be evaluated by

$$h^{jk}(t, R) = \frac{2G}{Rc^4} \ddot{Q}^{jk}, \tag{14}$$

where  $R$  is the distance between the source and the observer and, due to the above polarizations,  $\{j, k\} = 1, 2$ .

From equation (14), it is straightforward to show that, for a binary system where  $m \ll M$  and orbits have gravitomagnetic corrections, the Cartesian components of GW amplitude are

$$\begin{aligned}
h^{xx} &= 2\mu \left[ (3 \cos^2 \phi \sin^2 \theta - 1) \dot{r}^2 + 6r (\dot{\theta} \cos^2 \phi \sin 2\theta \right. \\
&\quad - \dot{\phi} \sin^2 \theta \sin 2\phi) \dot{r} + r \left( (3 \cos^2 \phi \sin^2 \theta - 1) \ddot{r} \right. \\
&\quad + 3r (\dot{\theta}^2 \cos 2\theta \cos^2 \phi - \dot{\phi} \dot{\theta} \sin 2\theta \sin 2\phi \\
&\quad - \sin \theta (\sin \theta (\dot{\phi}^2 \cos 2\phi + \ddot{\phi} \cos \phi \sin \phi) \\
&\quad \left. - \ddot{\theta} \cos \theta \cos^2 \phi) \right) \left. \right], \tag{15}
\end{aligned}$$

$$\begin{aligned}
h^{yy} &= 2\mu \left[ (3 \sin^2 \theta \sin^2 \phi - 1) \dot{r}^2 \right. \\
&\quad + 6r (\dot{\phi} \sin 2\phi \sin^2 \theta + \dot{\theta} \sin 2\theta \sin^2 \phi) \dot{r} \\
&\quad + r \left( (3 \sin^2 \theta \sin^2 \phi - 1) \ddot{r} + 3r (\dot{\theta}^2 \cos 2\theta \sin^2 \phi \right. \\
&\quad + \dot{\phi} \dot{\theta} \sin 2\theta \sin 2\phi + \sin \theta (\dot{\theta} \cos \theta \sin^2 \phi \\
&\quad \left. + \sin \theta (\dot{\phi}^2 \cos 2\phi + \ddot{\phi} \cos \phi \sin \phi) \right) \left. \right), \tag{16}
\end{aligned}$$

$$\begin{aligned}
h^{xy} &= h^{yx} = 3\mu \left[ \cos 2\phi \sin \theta (4\dot{\theta} \dot{\phi} \cos \theta + \ddot{\phi} \sin \theta) r^2 \right. \\
&\quad + 2\dot{r} (2\dot{\phi} \cos 2\phi \sin^2 \theta + \dot{\theta} \sin 2\theta \sin 2\phi) r \\
&\quad + \frac{1}{2} \sin 2\phi (2\ddot{r} \sin^2 \theta + r(t) (2\dot{\theta}^2 \cos 2\theta - 4\dot{\phi}^2 \sin^2 \theta \\
&\quad \left. + \dot{\theta} \sin 2\theta)) r + \dot{r}^2 \sin \theta \sin 2\phi \right], \tag{17}
\end{aligned}$$

where we are assuming geometrized units. The above formulas have been obtained from equations (6)–(8). The gravitomagnetic corrections give rise to signatures on the GW amplitudes that, in the standard Newtonian orbital motion, are not present (see for example [22, 23]). On the other hand, as discussed in the Introduction, such corrections cannot be discarded in peculiar situations such as dense stellar clusters or in the vicinity of galaxy central regions.

Finally, the expected dimensionless strain amplitude turns out to be  $h \simeq (h_{xx}^2 + h_{yy}^2 + 2h_{xy}^2)^{1/2}$ . In particular, considering a monochromatic GW, we have two independent degrees of freedom that, in the TT gauge, are  $h_+ = h_{xx} + h_{yy}$  and  $h_\times = h_{xy} + h_{yx}$ . We evaluate these quantities and the results are shown in figures 3–6.

#### 4.1. Numerical results

Now we have all the ingredients to estimate the effects of gravitomagnetic corrections on GW radiation. Calculations were performed in geometrized units in order to better evaluate relative corrections in the absence of gravitomagnetism. For numerical simulations, we assumed fiducial systems constituted by an  $m = 1.4M_\odot$  neutron star or an  $m = 10M_\odot$  massive stellar object orbiting around an MBH  $M \simeq 3 \times 10^6 M_\odot$  such as SgrA\*. In the extreme mass-ratio limit, this means that we can consider  $\mu = \frac{mM}{m+M}$  of about  $\mu \approx 1.4M_\odot$  and  $\mu \approx 10M_\odot$ . Computations were performed starting with orbital radii measured in the mass unit and scaling the distance according to the values shown in table 1. As seen in table 1, starting from  $r_0 = 20\mu$  up to  $2500\mu$ , the orbital eccentricity  $e = \frac{r_{\max} - r_{\min}}{r_{\max} + r_{\min}}$  evolves toward a circular orbit. In table 1, the GW frequencies, in mHz, as well as the dimensionless  $h$  amplitude strains and the two polarizations  $h_+$  and  $h_\times$  are shown. The values are the mean values of the GW dimensionless  $h$  amplitude strains ( $h = \frac{h_{\max} + h_{\min}}{2}$ ) and the maxima of the polarization waves (see figures 5 and 6). In figure 7, the fiducial LISA dimensionless  $h$  strains sensitivity curve is shown [5], considering the confusion noise produced by white dwarf binaries (blue curve). We also show the  $h$  dimensionless strains amplitudes (red diamond and green circles for  $\mu \approx 1.4M_\odot$  and  $\approx 10M_\odot$ , respectively). It is worth noting that, due to very high signal to noise ratio, the binary systems that we are considering are extremely interesting, in terms of probability detection, for the LISA interferometer (see figure 7).

#### 5. Event number estimations toward SgrA\*

At this point, it is important to give some estimates of the number of events where gravitomagnetic effects could be a signature for orbital motion and gravitational radiation. From the GW emission point of view, close orbital encounters, collisions and tidal interactions have to be dealt with on average if we want to investigate gravitational radiation in a dense stellar system. On the other hand, dense stellar regions are the favored target for the LISA interferometer [14]; hence it is extremely useful to provide suitable numbers before its launching.

To this end, it is worth giving the stellar encounter rate producing GWs in astrophysical systems such as dense

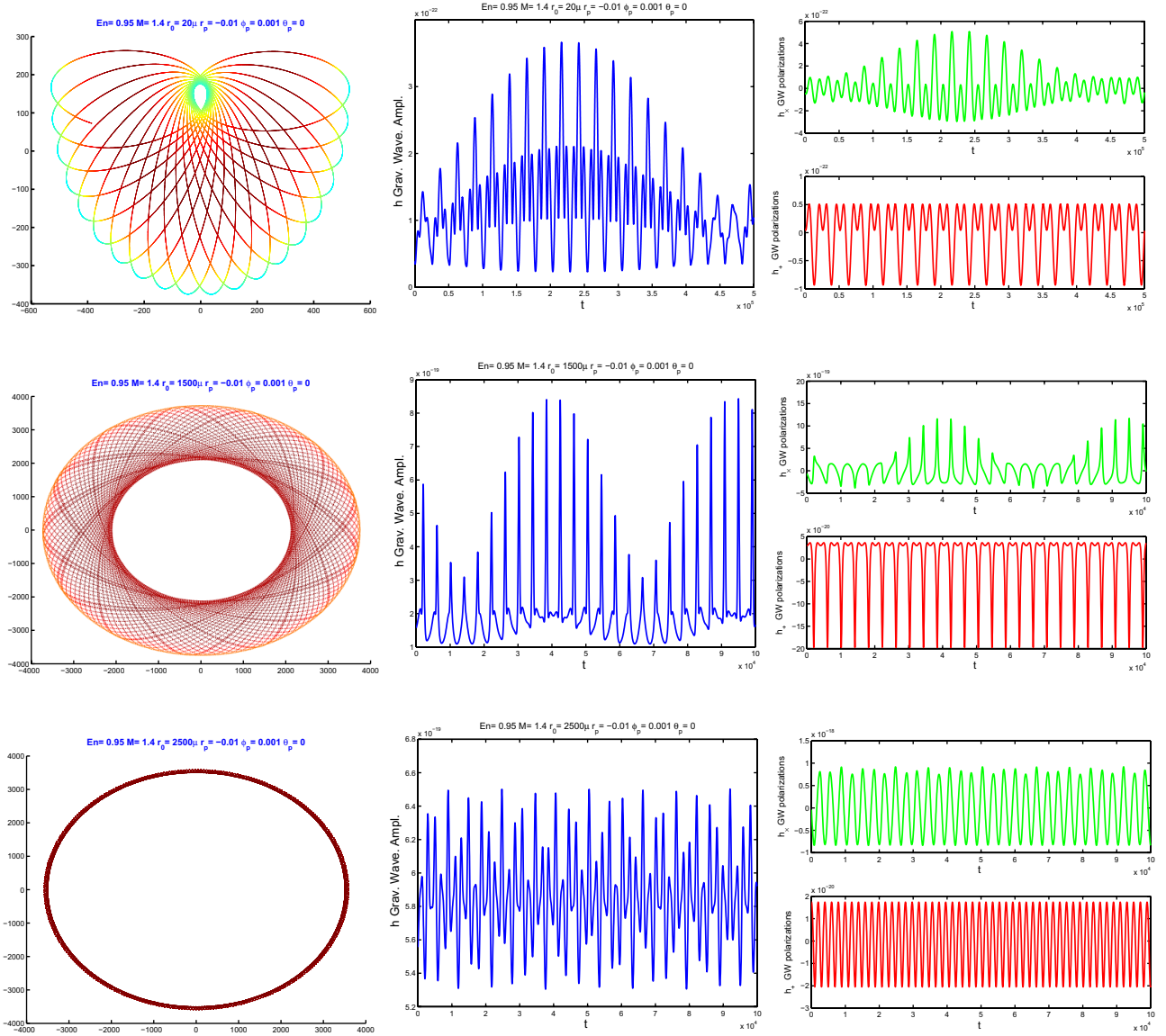


**Figure 5.** Plots along the panel line from left to right of velocities along the axes of maximal covariance, total gravitational emission waveform  $h$  and gravitational waveform polarizations  $h_+$  and  $h_x$  for a neutron star of  $1.4M_\odot$ . The waveform was computed for the Earth-distance from Sagittarius A (the central Galactic BH SgrA\*). The plots have been obtained by solving the system for the following parameters and initial conditions:  $\mu \approx 1.4M_\odot$ ,  $E = 0.95$ ,  $\phi_0 = 0$ ,  $\theta_0 = \frac{\pi}{2}$ ,  $\dot{\theta}_0 = 0$ ,  $\dot{\phi}_0 = -\frac{1}{10}\dot{r}_0$  and  $\dot{r}_0 = -\frac{1}{100}$ . From top to bottom of the panels, the orbital radius is  $r_0 = 20, 1500$  and  $2500\mu$ . See also table 1. The velocity field is represented ‘face-on’ along the axes of maximal covariance to better represent how gravitomagnetic corrections affect the phase space portrait of the system.

**Table 1.** GW amplitudes and frequencies as a function of eccentricity  $e$ , reduced mass  $\mu$  and orbital radius  $r_0$  for the two cases of fiducial stellar objects  $m \simeq 1.4M_\odot$  and  $m \simeq 10M_\odot$  orbiting around an MBH of mass  $M \simeq 3 \times 10^6M_\odot$ .

$r_0/\mu$	$e$	$f$ (mHz)	$1.4M_\odot$			$10M_\odot$				
			$h$	$h_+$	$h_x$	$e$	$f$ (mHz)	$h$	$h_+$	$h_x$
20	0.91	$7.7 \times 10^{-2}$	$2.0 \times 10^{-22}$	$5.1 \times 10^{-23}$	$5.1 \times 10^{-22}$	0.98	$3.2 \times 10^{-2}$	$1.5 \times 10^{-18}$	$1.6 \times 10^{-19}$	$4.3 \times 10^{-18}$
200	0.79	$1.1 \times 10^{-1}$	$1.2 \times 10^{-20}$	$2.2 \times 10^{-21}$	$3.1 \times 10^{-20}$	0.87	$9.2 \times 10^{-2}$	$1.5 \times 10^{-16}$	$2.5 \times 10^{-18}$	$4.1 \times 10^{-16}$
500	0.64	$1.4 \times 10^{-1}$	$6.9 \times 10^{-20}$	$8.7 \times 10^{-21}$	$1.7 \times 10^{-19}$	0.71	$1.4 \times 10^{-1}$	$8.5 \times 10^{-16}$	$7.0 \times 10^{-18}$	$2.4 \times 10^{-15}$
1000	0.44	$1.9 \times 10^{-1}$	$2.6 \times 10^{-19}$	$6.4 \times 10^{-20}$	$6.4 \times 10^{-19}$	0.49	$1.9 \times 10^{-1}$	$2.0 \times 10^{-15}$	$1.6 \times 10^{-17}$	$5.6 \times 10^{-15}$
1500	0.28	$2.3 \times 10^{-1}$	$4.8 \times 10^{-19}$	$3.6 \times 10^{-20}$	$1.2 \times 10^{-18}$	0.32	$2.3 \times 10^{-1}$	$2.7 \times 10^{-15}$	$2.5 \times 10^{-17}$	$7.4 \times 10^{-15}$
2000	0.14	$2.7 \times 10^{-1}$	$5.9 \times 10^{-19}$	$4.9 \times 10^{-20}$	$1.3 \times 10^{-18}$	0.19	$2.6 \times 10^{-1}$	$2.8 \times 10^{-15}$	$3.3 \times 10^{-17}$	$7.6 \times 10^{-15}$
2500	0.01	$3.1 \times 10^{-1}$	$5.9 \times 10^{-19}$	$1.7 \times 10^{-20}$	$9.2 \times 10^{-19}$	0.08	$2.9 \times 10^{-1}$	$2.1 \times 10^{-15}$	$4.0 \times 10^{-17}$	$5.6 \times 10^{-15}$

globular clusters or the Galactic Center. In general, stars are approximated as point masses. However, in dense regions of stellar systems, stars can pass so close to another that they

raise tidal forces that dissipate their relative orbital kinetic energy and Newtonian mechanics or the weak field limit of GR cannot be adopted as good approximations. In some cases,

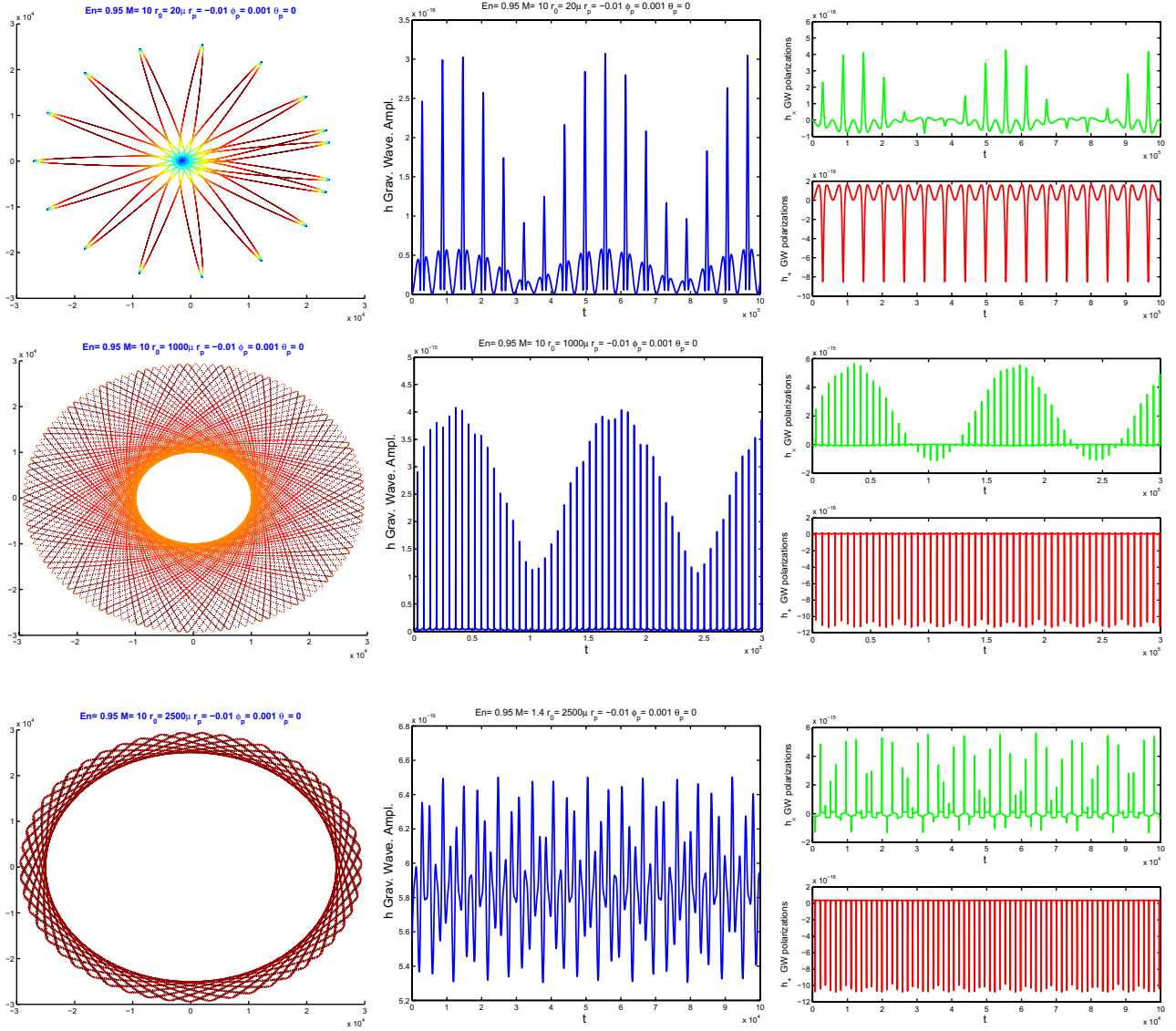


**Figure 6.** Plots along the panel lines from left to right of velocities along the axes of maximal covariance, total gravitational emission waveform  $h$  and gravitational waveform polarizations  $h_+$  and  $h_\times$  for a BH of  $10M_\odot$ . The waveform was computed for the Earth-distance to SgrA\*. The plots we show have been obtained solving the system for the following parameters and initial conditions:  $\mu \approx 10M_\odot$ ,  $E = 0.95$ ,  $\phi_0 = 0$ ,  $\theta_0 = \frac{\pi}{2}$ ,  $\dot{\theta}_0 = 0$ ,  $\dot{\phi}_0 = -\frac{1}{10}\dot{r}_0$  and  $\dot{r}_0 = -\frac{1}{100}$ . From top to bottom of the panels, the orbital radius is  $r_0 = 20$ , 1000 and 2500  $\mu$ . See also table 1. The field of velocities is represented ‘face-on’ along the axes of maximal covariance to better represent how gravitomagnetic corrections affect the phase space portrait of the system.

the loss of energy can be so large that stars form binary (the situation that we have considered here) or multiple systems; in other cases, stars collide and coalesce into a single star; finally stars can exchange gravitational interaction in non-returning encounters.

To investigate and parameterize all these effects, one has to compute the collision time  $t_{\text{coll}}$ , where  $1/t_{\text{coll}}$  is the collision rate, that is, the average number of physical collisions that a given star suffers per unit time. As a rough approximation, one can restrict oneself to stellar clusters in which all stars have the same mass  $m$ .

Let us consider an encounter with initial relative velocity  $\mathbf{v}_0$  and impact parameter  $b$ . The angular momentum per unit mass of the reduced particle is  $L = bv_0$ . At the distance of closest approach, which we denote by  $r_{\text{coll}}$ , the radial velocity must be zero, and hence the angular momentum is  $L = r_{\text{coll}}v_{\text{max}}$ , where  $v_{\text{max}}$  is the relative speed at  $r_{\text{coll}}$ . It is easy

to show that [17]

$$b^2 = r_{\text{coll}}^2 + \frac{4Gmr_{\text{coll}}}{v_0^2}. \quad (18)$$

If we set  $r_{\text{coll}}$  equal to the sum of the radii of the two stars, a collision will occur if the impact parameter is less than the value of  $b$ , as determined by equation (18).

The function  $f(\mathbf{v}_a)d^3\mathbf{v}_a$  gives the number of stars per unit volume with velocities in the range  $\mathbf{v}_a + d^3\mathbf{v}_a$ . The number of encounters per unit time with impact parameter less than  $b$ , which are suffered by a given star, is  $f(\mathbf{v}_a)d^3\mathbf{v}_a$  times the volume of the annulus with radius  $b$  and length  $v_0$ , that is

$$\int f(\mathbf{v}_a)\pi b^2 v_0 d^3\mathbf{v}_a, \quad (19)$$

where  $v_0 = |\mathbf{v} - \mathbf{v}_a|$  and  $\mathbf{v}$  is the velocity of the considered star. The quantity in equation (19) is equal to  $1/t_{\text{coll}}$  for a star

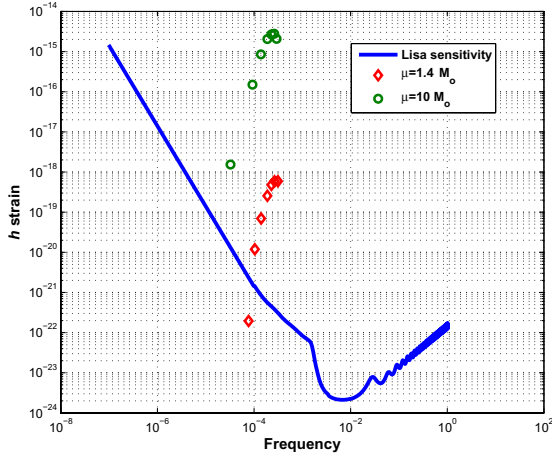


**Figure 7.** Plot of estimated mean values of GW emission in terms of dimensionless strain  $h$  for two binary sources at the Galactic Center SgrA\* with reduced mass  $\mu \approx 1.4M_\odot$  (red diamonds) and  $\mu \approx 10M_\odot$  (green circles). The blue line is the foreseen LISA dimensionless  $h$  strains sensitivity curve. The waveforms were computed for the Earth-distance to SgrA\*. The examples we show have been obtained by solving the system for the parameters and initial conditions reported in figures 5 and 6 and in table 1. It is worth noting that we are considering here that the dimensionless strain amplitudes and typical durations can be computed according to figure 4. They are of the order  $10^7$ – $10^8$  s.

with velocity  $\mathbf{v}$ : to obtain the mean value of  $1/t_{\text{coll}}$ , we average over  $\mathbf{v}$  by multiplying (19) by  $f(\mathbf{v})/v$ , where  $v = \int f(\mathbf{v}) d^3\mathbf{v}$  is the number density of stars and integration is over  $d^3\mathbf{v}$ . Thus

$$\frac{1}{t_{\text{coll}}} = \frac{v}{8\pi^2\sigma^6} \int e^{-(v^2+v_a^2)/2\sigma^2} \times \left( r_{\text{coll}}|\mathbf{v} - \mathbf{v}_a| + \frac{4Gmr_{\text{coll}}}{|\mathbf{v} - \mathbf{v}_a|} \right) d^3\mathbf{v} d^3\mathbf{v}_a. \quad (20)$$

Replacing the variable  $\mathbf{v}_a$  by  $\mathbf{V} = \mathbf{v} - \mathbf{v}_a$ , the argument of the exponential is then  $-[(\mathbf{v} - \frac{1}{2}\mathbf{V})^2 + \frac{1}{4}V^2]/\sigma^2$ , and if we replace the variable  $\mathbf{v}$  by  $\mathbf{v}_{\text{cm}} = \mathbf{v} - \frac{1}{2}\mathbf{V}$  (the center of mass velocity), then one has

$$\frac{1}{t_{\text{coll}}} = \frac{v}{8\pi^2\sigma^6} \int e^{-(v_{\text{cm}}^2+V^2)/2\sigma^2} \left( r_{\text{coll}}V + \frac{4Gmr_{\text{coll}}}{V} \right) dV. \quad (21)$$

The integral over  $\mathbf{v}_{\text{cm}}$  is given by

$$\int e^{-v_{\text{cm}}^2/\sigma^2} d^3\mathbf{v}_{\text{cm}} = \pi^{3/2}\sigma^3. \quad (22)$$

Thus

$$\frac{1}{t_{\text{coll}}} = \frac{\pi^{1/2}v}{2\sigma^3} \int_0^\infty e^{-V^2/4\sigma^2} (r_{\text{coll}}^2 V^3 + 4GmVr_{\text{coll}}) dV. \quad (23)$$

The integrals can be easily calculated and then we find

$$\frac{1}{t_{\text{coll}}} = 4\sqrt{\pi}v\sigma r_{\text{coll}}^2 + \frac{4\sqrt{\pi}vGmr_{\text{coll}}}{\sigma}. \quad (24)$$

The first term of this result can be derived from kinetic theory. The rate of interaction is  $v\Sigma\langle V \rangle$ , where  $\Sigma$  is the cross-section and  $\langle V \rangle$  is the mean relative speed. Substituting  $\Sigma = \pi r_{\text{coll}}^2$  and  $\langle V \rangle = 4\sigma/\sqrt{\pi}$  (which is appropriate for a Maxwellian

distribution with dispersion  $\sigma$ ), we recover the first term of (24). The second term represents the enhancement in the collision rate by gravitational focusing, that is, the deflection of trajectories by the gravitational attraction of the two stars.

If  $r_*$  is the stellar radius, we may set  $r_{\text{coll}} = 2r_*$ . It is convenient to introduce the escape speed from the stellar surface,  $v_* = \sqrt{2Gm/r_*}$ , and to rewrite equation (24) as

$$\Gamma = \frac{1}{t_{\text{coll}}} = 16\sqrt{\pi}v\sigma r_*^2 \left( 1 + \frac{v_*^2}{4\sigma^2} \right) = 16\sqrt{\pi}v\sigma r_*^2 (1 + \Theta), \quad (25)$$

where

$$\Theta = \frac{v_*^2}{4\sigma^2} = \frac{Gm}{2\sigma^2 r_*} \quad (26)$$

is the Safronov number [17]. In evaluating the rate, we consider only those encounters producing GWs, for example, in the LISA range, i.e. between  $10^{-4}$  and  $10^{-1}$  Hz (see e.g. [28]). Numerically, we have

$$\Gamma \simeq 5.5 \times 10^{-10} \left( \frac{v}{10 \text{ km s}^{-1}} \right) \left( \frac{\sigma}{UA^2} \right) \left( \frac{10 \text{ pc}}{R} \right)^3 \text{ year}^{-1} \quad (27)$$

$$\Theta \ll 1,$$

$$\Gamma \simeq 5.5 \times 10^{-10} \left( \frac{M}{10^5 M_\odot} \right)^2 \left( \frac{v}{10 \text{ km s}^{-1}} \right) \times \left( \frac{\sigma}{UA^2} \right) \left( \frac{10 \text{ pc}}{R} \right)^3 \text{ years}^{-1} \quad \Theta \gg 1. \quad (28)$$

If  $\Theta \gg 1$ , the energy dissipated exceeds the relative kinetic energy of the colliding stars, and the stars coalesce into a single star. This new star may, in turn, collide and merge with other stars, thereby becoming very massive. As its mass increases, the collision time is shortened and then there may be runaway coalescence leading to the formation of a few supermassive objects per cluster. If  $\Theta \ll 1$ , much of the mass in the colliding stars may be liberated and forming new stars or single supermassive objects (see [29, 30]). Both cases are interesting for LISA purposes.

Note that when one has the effects of quasi-collisions (where gravitomagnetic effects, in principle, cannot be discarded) in an encounter of two stars in which the minimal separation is several stellar radii, violent tides will be raised on the surface of each star. The energy that excites the tides comes from the relative kinetic energy of the stars. This effect is important for  $\Theta \gg 1$  because the loss of a small amount of kinetic energy may leave the two stars with negative total energy, that is, as a bounded binary system. Successive peri-center passages will dissipate more energy by GW radiation, until the binary orbit is nearly circular with negligible or null GW radiation emission.

Let us apply these considerations to the Galactic Center, which can be modeled as a system of several compact stellar clusters, some of them similar to very compact globular clusters with high emission in x-rays [31].

For a typical globular cluster around the Galactic Center, the expected event rate is of the order of  $2 \times 10^{-9} \text{ years}^{-1}$ , which may be increased at least by a factor  $\simeq 100$  if one considers the number of globular clusters in the whole Galaxy.

If the stellar cluster at the Galactic Center is taken into account and assuming the total mass  $M \simeq 3 \times 10^6 M_\odot$ , the velocity dispersion  $\sigma \simeq 150 \text{ km s}^{-1}$  and the radius of the object  $R \simeq 10 \text{ pc}$  (where  $\Theta = 4.3$ ), one expects to have  $\simeq 10^{-5}$  open orbit encounters per year. On the other hand, if a cluster with total mass  $M \simeq 10^6 M_\odot$ ,  $\sigma \simeq 150 \text{ km s}^{-1}$  and  $R \simeq 0.1 \text{ pc}$  is considered, an event rate number of the order of unity per year is obtained. These values could be realistically achieved by data coming from the forthcoming space interferometer LISA. As a secondary effect, the above waveforms could constitute the ‘signature’ to classify the different stellar encounters thanks to the differences of the shapes (see figures 5 and 6).

## 6. Conclusions

In this paper, we have discussed gravitomagnetic effects on orbital motions that could give rise to interesting phenomena in tight binding systems such as binaries of evolved objects (neutron stars or BHs). The effects become particularly relevant when such objects orbit around or fall toward very MBHs such as those at the center of galaxies. The effects are particularly interesting if  $v/c$  is in the range  $(10^{-1} - 10^{-4})c$ . Gravitomagnetic orbital corrections, after long integration time, can induce precession and nutation effects capable of affecting the stability basin of the orbits. The global structure of such a basin is extremely sensitive to initial radial velocities and angular velocities, initial energy and masses, which can determine possible transitions to chaotic behavior. In principle, GW emission could present signatures of gravitomagnetic corrections after suitable integration times, in particular for the ongoing LISA space laser interferometric GW antenna.

Some remarks on the detectability of such effects are necessary at this point. In a first scenario, the detection could be possible by ignoring gravitomagnetic corrections at the beginning. In this case, the presence of such corrections could be investigated in a post-detection analysis. This strategy means that a very fine off-line data reduction should be pursued to test the presence of the effects. From a genuine physical viewpoint, offline analysis means that a clear theoretical classification of waveforms and signatures of various phenomena is necessary. A second possibility could be on-line detection. In such a case, suitable templates for the signals should be available and then a preliminary classification is necessary. It is worth stressing that the two strategies are very different. In the first case, gravitomagnetic effects can be seen as ‘anomalies’ or ‘corrections’ on the standard templates adopted for detection. In the second case, a fine theoretical study is necessary ‘a priori’ in order to produce suitable templates. In other words, the first approach seems more operative while the second seems more correct. However, these preliminary considerations have to be supported by a robust theoretical analysis of dynamics around systems such as the MBHs that we have taken into account [14]. A third strategy is also possible, i.e. a blind search using adaptive filters such as the infinite impulse response adaptive line enhancer (the so-called IIR ALE for blind detection of GWs [32, 33]). Clearly, the signature for gravitomagnetic effects emerges as soon as dynamics is going

to become critical and the standard weak field and slow motion approximations fail in giving an accurate description of phenomena. These will be the arguments of forthcoming studies.

## References

- [1] Abramovici A *et al* 1992 *Science* **256** 325 Online at <http://www.ligo.org>
- [2] Caron B *et al* 1997 *Class. Quantum Gravity* **14** 1461 Online at <http://www.virgo.infn.it>
- [3] Luck H *et al* 1997 *Class. Quantum Gravity* **14** 1471 Online at <http://www.geo600.uni-hannover.de>
- [4] Ando M *et al* 2001 *Phys. Rev. Lett.* **86** 3950 Online at <http://tamago.mtk.nao.ac.jp>
- [5] <http://www.lisa-science.org>
- [6] Poisson E 2004 *Living Rev. Rel.* **6** 3 <http://relativity.livingreviews.org>
- [7] Mino Y 2005 *Prog. Theor. Phys.* **113** 733  
Mino Y 2006 *Prog. Theor. Phys.* **115** 43  
Pound A, Poisson E and Nickel B G 2005 *Phys. Rev. D* **72** 124001  
Barack L and Lousto C 2005 *Phys. Rev. D* **72** 104026  
Barack L and Sago N 2007 *Phys. Rev. D* **75** 064021
- [8] Finn L S and Thorne K S 2000 *Phys. Rev. D* **62** 124021  
Babak S *et al* 2007 *Phys. Rev. D* **75** 024005  
Sigl G, Schnittman J and Buonanno A 2007 *Phys. Rev. D* **75** 024034
- [9] Viollier R D 1994 *Prog. Part. Nucl. Phys.* **32** 51
- [10] Capozziello S and Iovane G 1999 *Phys. Lett. A* **259** 185
- [11] Sigurdsson S and Rees M 1997 *Mon. Not. R. Astron. Soc.* **284** 318
- [12] Sigurdsson S 1997 *Class. Quantum Grav.* **14** 1425
- [13] Danzmann K *et al* 1998 LISA-Laser Interferometer Space Antenna, Pre-Phase A Report, Max-Planck-Institut für Quantenoptik, Report MPQ 233
- [14] Amaro-Seoane P *et al* 2007 *Class. Quantum Gravity* **24** R113
- [15] Capozziello S, De Laurentis M, Garufi F and Milano L 2009 *Phys. Scr.* **79** 025901
- [16] <http://www.wolfram.com>
- [17] Binney J and Tremaine S 1987 *Galactic Dynamics* (Princeton: Princeton University Press)
- [18] Landau L and Lifshits E M 1973 *Mechanics* (New York: Pergamon)
- [19] Thirring H 1918 *Phys. Z* **19** 204
- [20] Thirring H 1918 *Phys. Z* **19** 33  
Thirring H 1921 *Phys. Z* **22** 29  
Lense J and Thirring H 1918 *Phys. Z* **19** 156  
Mashhoon B, Hehl F W and Theiss D S 1984 *Gen. Rel. Grav.* **16** 711 (Engl. Transl.)
- [21] Ryan F D 1997 *Phys. Rev. D* **56** 1845
- [22] Capozziello S and De Laurentis M 2008 *Astropart. Phys.* **30** 105
- [23] Capozziello S, De Laurentis M, De Paolis F, Ingrassio G and Nucita A 2008 *Mod. Phys. Lett. A* **23** 99
- [24] Barack L and Cutler C 2004 *Phys. Rev. D* **69** 082005
- [25] Barack L and Cutler C 2004 *Phys. Rev. D* **70** 122002
- [26] Freitag M 2003 *Astro. Phys. J.* **583** L21
- [27] Capozziello S, De Laurentis M and Francaviglia M 2008 *Astropart. Phys.* **29** 125
- [28] Rubbo L J, Holley-Bockelmann K and Finn L S 2006 *Astrophys. J.* **649** L25
- [29] Belgeman M C and Rees M J 1978 *Mon. Not. R. Astron. Soc.* **185** 847
- [30] Lightman A P and Shapiro S L 1978 *Rev. Mod. Phys.* **50** 437
- [31] Genzel R and Townes C H 1987 *Ann. Rev. Astron. Astrophys.* **25** 1
- [32] Milano L, Barone F and Milano M 1997 *Phys. Rev. D* **55** 4537
- [33] Eleuteri A, Milano L, De Rosa R and Garufi F 2006 *Phys. Rev. D* **73** 122004